not kinetic, phases. In the case of stoichiometric reactions, the thermodynamic product forcibly has the same stoichiometry as the ternary reagent, since the product lattices are so much more energetically favorable than the reagent lattices. In nonstoichiometric reactions like (1), free non-metal byproducts are also produced, and their presence is a complication. The different volatilities of S and Se, not only in the solid-solution product but also from the free elements, bring about changes in the composition of the final product at different temperatures. The final product is therefore dependent upon the relative bond strengths between the metal and the competing non-metal components, their volatilities, and the thermal treatment of the reaction once it has reached equilibrium at a specific temperature and pressure. The study of a solid–gas equilibrium for such a system is a formidable task. The above modifications therefore address the problems associated with the presence of excess chalcogen and the unequal diffusion rates of competing non-metals leading to preferential enrichment, compositional gradients, and variable stoichiometry.

The solid-state, solid-solution-precursor approach is also applicable to other mixed-anion systems. Experiments with metal mixed-pnictide and metal chalcogenide/pnictide systems are in progress. Alkali-metal mixed pnictides, such as $Na_3(P,As)$ and $Na_3(As,Sb)$, are prepared by heating their constituent elements at moderate temperatures. Like their mixed-chalcogenide analogues, they can be more safely manipulated than the corresponding gases, phosphine or arsine. They are then reacted with a large number of main-group and rare-earth metals to produce compounds such as Ga(P,As) or Gd(P,As).[29]

Conclusions

Experiments with binary group VI transition-metal dichalcogenides illustrate that part of the mechanism in these self-sustaining, solid-state precursor reactions appears to involve elemental intermediates that are the result of a powerful redox process. The high reaction temperatures generated promote reaction between the elements to form product. As is the case with most solid-state reactions, diffusion is a very important consideration. Any factors favoring diffusion, such as smaller reagent particle sizes or more intimate mixing, higher temperatures, and longer heating times, also favor products. The proposed mechanistic arguments are further supported by experiments with molybdenum and tungsten mixed-anion dichalcogenides. The phenomena of selective enrichment, compositional gradients, and variable stoichiometry in the products are readily explained by the competitive diffusion of different non-metals under reaction conditions of rapid, nonuniform heating and quick cooling.

Acknowledgment. This work was supported by National Science Foundation Grant No. CHE 8657822 through the Presidential Young Investigator Award Program along with matching funds provided by the Ford Motor Co. and a David and Lucille Packard Foundation Fellowship in Science and Engineering.

(29) Treece, R. E.; Kaner, R. B. *Chem. Mater.*, to be submitted for publication.

Contribution from the Dipartimento di Chimica, Università di Firenze, and Istituto per lo Studio della Stereochemica ed Energetica dei Composti di Coordinazione, Firenze, Italy

Electronic Structure and Magnetic Properties of the Hexanuclear Octahedral Cluster $[Co_6(\mu_3\text{-}S)_8(PEt_3)_6]BPh_4$

Alessandro Bencini,* Stefano Midollini, and Claudia Zanchini

Received July 19, 1991

Single-crystal EPR spectra of the paramagnetic complex $[Co_6(\mu_3\text{-}S)_8(PEt_3)_6]BPh_4$ (PEt_3 = triethylphosphine; BPh_4 = tetraphenylborato anion) at 4.2 K were interpreted using a $S = {}^1/_2$ spin Hamiltonian with $g_x = 2.35$ (1), $g_y = 2.04$ (1), and $g_z = 1.95$ (1). The x, y, and z axes are close to the bond directions of one of the six inequivalent cobalt atoms. The compound is EPR silent at room temperature, both in the solid state and in solution. The temperature dependence of the intensity of the EPR signal is ascribed to a localization of the unpaired electron on one cobalt nucleus. The angular dependence of the peak-to-peak line width of the 4.2 K EPR signal seems to indicate the existence of a feeble magnetic interaction between the clusters in the solid state.

Introduction

Oligonuclear complexes of transition metals have attracted the interest of the scientific community for a long time, since they form the natural union between molecular and solid-state chemistry.[1] Agglomerates of metals have been found in naturally occurring enzymes, such the iron–sulfur proteins, as well as in pure inorganic solids,[2] and a large part of inorganic chemistry has recently been devoted to the synthesis of new types of clusters and to the development of theoretical methods for the calculation of their electronic structure.[3] Sulfide-containing minerals probably represent the best known naturally occurring inorganic systems in which aggregates of metals are present.[4] Some of these minerals offer peculiar physical properties arising from the fact that the metal–sulfur clusters are extensively interconnected to form extended structures. The best known substances of this type are probably the Chevrel phases of the molybdenum chalcogenides,[5] which include high-temperature and high-field superconductors.[6,7] The core of these solids is formed by a Mo_6X_8 (X = S, Se, Te, halogen) cluster in which an octahedron of six molybdenum atoms is encased in a cube of X atoms, and their electronic structure has been widely described using extended Hückel (EH) calculations.[8]

S.M. has reported the synthesis and the crystallographic characterization of a series of complexes of general formula $[M_6(\mu_3\text{-}S)_8(PEt_3)_6]^{n+}$, where M is cobalt or iron and n ranges from

(1) Lee, S. C.; Holm, R. H. *Angew. Chem., Int. Ed. Engl.* **1990**, *29*, 840.
(2) Johnson, M. K.; King, R. B.; Kurtz, D. M., Jr.; Kutal, C.; Norton, M. L.; Scott, R. A. *Electron Transfer in Biology and the Solid State*; American Chemical Society: Washington, DC, 1990.
(3) Selected references: (a) Simon, A. *Angew. Chem., Int. Ed. Engl.* **1981**, *20*, 1. (b) Christou, G. K.; Hagen, S.; Bashkin, J. K.; Holm, R. H. *Inorg. Chem.* **1985**, *24*, 1010. (c) Simon, A. *Angew. Chem., Int. Ed. Engl.* **1988**, *100*, 163. (d) Brennan, J. G.; Siegrist, T.; Stuczynski, M.; Steigerwald, M. L. *J. Am. Chem. Soc.* **1989**, *111*, 9240. (e) Wheeler, R. A. *J. Am. Chem. Soc.* **1990**, *112*, 8737. (f) Hoffman, G. G.; Bashkin, J. K.; Karplus, M. *J. Am. Chem. Soc.* **1990**, *112*, 8705. (g) Burdett, J. K.; Miller, G. J. *J. Am. Chem. Soc.* **1987**, *109*, 4081. (h) Albright, T. A.; Burdett, J. K.; Whangbo, M. H. *Orbital Interactions in Chemistry*; John Wiley & Sons: New York, 1985.
(4) Wells, A. F. *Structural Inorganic Chemistry*; Clarendon Press: Oxford, U.K., 1962.
(5) Chevrel, R.; Sergent, M.; Prigent, J. *J. Solid State Chem.* **1971**, *3*, 515.
(6) Fisher, O. *Appl. Phys.* **1978**, *16*, 1.
(7) Chevrel, R. In *Superconductor Materials Science: Metallurgy, Fabrication and Applications*; Foner, S., Schwartz, B. B., Eds.; Plenum Press: New York, 1981.
(8) Hughbanks, T.; Hoffmann, R. *J. Am. Chem. Soc.* **1983**, *105*, 1150.

0020-1669/92/1331-2132$03.00/0

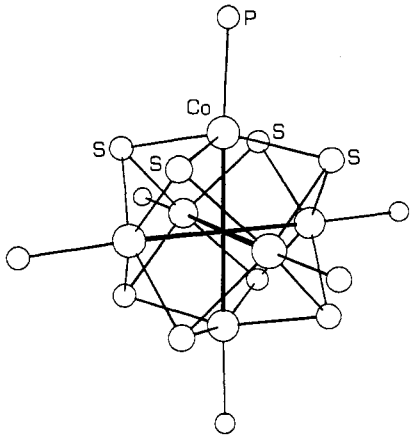

Figure 1. Schematic view of the room-temperature structure of the $[Co_6(\mu_3\text{-}S)_8P_6]^+$ cation.[9]

0 to 2.[9] Clusters with the same stoichiometry, but with different charges have been obtained electrochemically, but these have not yet been isolated in the solid state. When M is Co, for example, only compounds with $n = 0$ and $n = 1$ have been obtained as stable products, while oxidation states with $n = 2$ and 3 have been found in the electrochemical cell, and the −1 state has never been observed. All the complexes so far isolated are isostructural and contain a quasi-regular octahedron of M atoms, each atom being coordinated by four basal sulfurs and one axial phosphorus in a distorted square pyramidal environment. The eight sulfur atoms form a distorted cube. The highest crystallographic symmetry was found[10] to be S_6 ($C_3 \otimes i$) in the complex $[Fe_6(\mu_3\text{-}S)_8(PEt_3)_6]PF_6$. A schematic view of the $[Co_6S_8P_6]^+$ cation is shown in Figure 1. The structural similarity between these complexes and the Chevrel phases as well as their difference is apparent; namely, they have the octahedron of metals encased in a cube of sulfur atoms but possess an axial PEt_3 ligand which, at a first glance, prevents the formation of spatially extended structures. These systems, therefore, seem to be good candidates for the investigation of the molecular and electronic structure of the "isolated" $[M_6S_8]^{n+}$ moieties. More recently, molecular clusters of formula $[Mo_6(\mu_3\text{-}S)_8(PEt_3)_6]^{0,-}$ have also been synthesized and structurally characterized.[11]

We wish to report here the single-crystal EPR spectra and the magnetic properties of the paramagnetic complex $[Co_6(\mu_3\text{-}S_8)(PEt_3)_6]BPh_4$.

Experimental Section

Synthesis of the Complex. The complex $[Co_6(\mu_3\text{-}S)_8(PEt_3)_6]BPh_4$ was prepared as previously reported.[9] Single crystals suitable for EPR spectroscopy were grown from a dichloromethane–1-butanol solution, by slow evaporation of the solvent.

EPR Spectra. Single crystals of $[Co_6(\mu_3\text{-}S)_8(PEt_3)_6]BPh_4$ were found to conform to the structure report[9] using a Philips PW1100 automated diffractometer. The crystals are triclinic, of space group $P\bar{1}$, with cell dimensions $a = 1948.1$ pm, $b = 1556.2$ pm, $c = 1239.0$ pm, $\alpha = 92.7°$, $\beta = 94.5°$, and $\gamma = 94.1°$. For the EPR measurements, crystals larger than those previously used for the structure determination were required. The growing procedure yielded sufficiently large crystals, but in each case they exhibited the X-ray diffusion pattern characteristic of twinned crystals with diffuse peaks having broad profiles.

Single-crystal and fluid-solution EPR spectra were measured at variable temperature between 300 and 4.2 K using a Varian E-9 spectrometer equipped with an Oxford Instruments continuous-flow cryostat. Fluid- and frozen-solution spectra were measured on $\approx 10^{-4}$ M solutions of the complex in CH_2Cl_2 and in acetone. The choice of these solvents was imposed by the insolubility of the present compound in apolar organic solvents. In order to improve the quality of the frozen-solution spectra and to obtain a satisfactory glass, DMF and dimethyl sulfoxide were also employed. In each case, no signal was detected at temperatures higher than 20 K.

Single-crystal spectra were measured by rotating the crystals around the orthogonal axes X, Y, Z, with $Z \equiv c$ and $X \equiv a^*$. The angle between a and X is 6.2°, and that between b and Y is 2.7°.

NMR Spectra. ^1H NMR spectra were obtained for $[Co_6(\mu_3\text{-}S)_8(PEt_3)_6]BF_4$ at room temperature by using a Varian XR 300 spectrometer.

Calculations. All calculations were performed on an IBM Personal System/2 80/111 computer, using the procedures described later in the text.

Magnetic Measurements. The temperature dependence of the magnetic susceptibility was measured with an automated Faraday type magnetometer equipped with an Oxford Instruments continuous-flow cryostat operating in the temperature range 1.8–300 K. The diamagnetic correction applied was 1045×10^{-6} emu mol^{-1} G^{-1}.

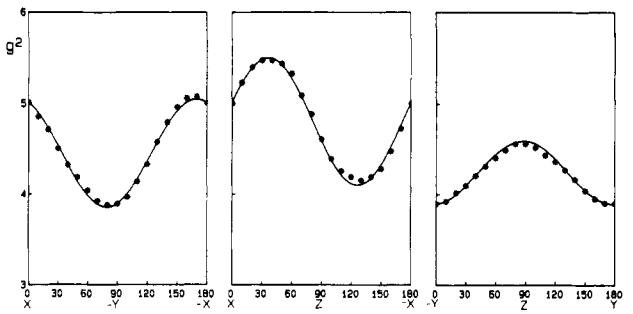

Figure 2. Angular dependence of g^2, measured at 4.2 K, for $[Co_6(\mu_3\text{-}S)_8(PEt_3)_6]BPh_4$ in the planes perpendicular to Z, Y, and X, respectively. The solid lines represent the best fit curves.

Table I. Principal Values and Directions[a] of the 4.2 K **g** Tensor of $[Co_6(\mu_3\text{-}S)_8(PEt_3)_6]BPh_4$ in the XYZ Reference Frame

	principal values	principal directions			molecular axes[b]
g_1	1.95 (1)	0.33 (4)	−0.89 (4)	−0.32 (7)	z
g_2	2.04 (1)	0.48 (3)	0.45 (8)	−0.75 (3)	y
g_3	2.35 (1)	0.81 (1)	0.09 (3)	0.58 (2)	x

[a] Direction cosines with respect to the X, Y, and Z laboratory axes. [b] See test for the labeling of the tensor axes.

Results

The cluster $[Co_6(\mu_3\text{-}S)_8(PEt_3)_6]^+$ possesses no crystallographic symmetry elements.[9] The relevant interatomic and bond distances are Co–Co = 279.4 (2) pm, Co–S = 223.4 (2) pm, and Co–P = 216.2 (2) pm. The cobalt and phosphorus atoms lie, within experimental error, on the vertices of a perfect octahedron, so that the cluster is quasi-centrosymmetric, with couples of bond distances and angles equal to each other, also within experimental error.

$[Co_6(\mu_3\text{-}S)_8(PEt_3)_6]BPh_4$ is EPR silent at room temperature both in the solid state and in solution. No signal was detected in any case at temperatures higher than 20 K. In the single crystal, only one signal was observed, below $\approx$20 K, for any crystal orientation. This signal sharpens upon cooling to 4.2 K. All single-crystal spectra were thus recorded at liquid-helium temperature. The observed angular dependence of the $\mathbf{g}^2$ tensor measured with the static magnetic field in the plane perpendicular to Z, Y, and X, respectively, is shown in Figure 2. The data were fitted using a $S = {}^1/_2$ spin Hamiltonian with a least-squares fitting procedure based on the Schönland method.[12] The principal values and directions of the **g** tensor are listed in Table I. The line shape of the signals was found to be asymmetric in almost all angular settings, and in some orientations two separate signals of different intensities or a shoulder on the main line was observed. The relative intensities of the two signals depend on the crystal dimensions as well as on the orientation in the static magnetic field, and they arise from the twinning of the crystals required for the EPR study (see Experimental Section). The data reported in

(9) (a) Cecconi, F.; Ghilardi, C. A.; Midollini, S.; Orlandini, A. *Inorg. Chim. Acta* **1982**, *64*, 147. (b) Cecconi, F.; Ghilardi, C. A.; Midollini, S.; Orlandini, A.; Zanello, P. *Polyhedron* **1986**, *5*, 2021.
(10) Cecconi, F.; Ghilardi, C. A.; Midollini, S.; Orlandini, A.; Zanello, P. *J. Chem. Soc., Dalton Trans.* **1987**, 831.
(11) Saito, T.; Yamamoto, N.; Nagase, T.; Tsuboi, T.; Kobayashi, K.; Yamagata, T.; Imoto, H.; Unoura, K. *Inorg. Chem.* **1990**, *29*, 764.
(12) Schönland, R. S. *Proc. Phys. Soc., London* **1959**, *73*, 788.

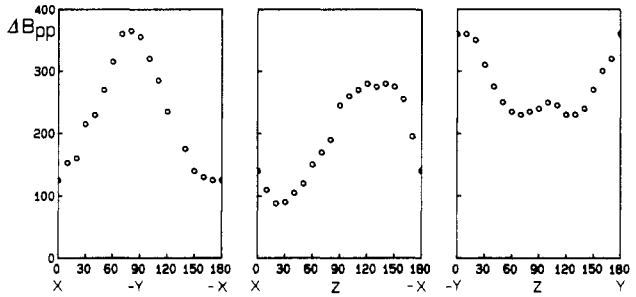

Figure 3. Observed angular dependence of ΔB_{pp} (gauss) of the ESR signal of $[Co_6(\mu_3\text{-}S)_8(PEt_3)_6]BPh_4$ in the planes perpendicular to Z, Y, and X, respectively.

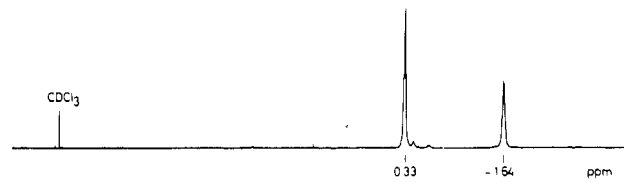

Figure 4. ^1H NMR spectrum of $[Co_6(\mu_3\text{-}S)_8(PEt_3)_6]BF_4$ in $CDCl_3$ solution at 293 K. Chemical shifts (δ) are indicated.

Figure 2 refer to the more intense feature.

The observed angular dependence of the peak-to-peak line width of the signal, ΔB_{pp}, is reported in Figure 3. The line width has a maximum roughly along the Y axis, corresponding to the highest field feature at $g = 1.97$ (1), and a minimum along the $X \equiv a^*$ axis, corresponding to the lowest field feature at $g = 2.24$ (1). In the YZ plane, a different line width behavior is observed, with a maximum close to Y ($5 \pm 10°$), a relative minimum $\approx 60°$ from it, and a second relative maximum close to $Z \equiv c$ ($5 \pm 10°$).

The temperature dependence of the solution EPR spectra is similar to the temperature dependence of the single-crystal spectra, since signals were observed only below ≈ 20 K. The 4.2 K spectra are similar to the polycrystalline-powder spectra and show very broad features characteristic of a rhombic $S = {}^1/_2$ spin system with unresolved hyperfine splitting.

The ^1H NMR spectrum of $[Co_6(\mu_3\text{-}S)_8(PEt_3)_6]^+$ is shown in Figure 4. It reveals slightly broadened, isotropically shifted signals for the methyl group at 0.33 ppm (t, 3 H), and for the methylene group at −1.64 ppm (q, 2 H). It is worth noting that, despite the paramagnetic nature of the compound, the H–H coupling was retained, with a value of $^3J_{H\text{-}H} = 7$ Hz, while no coupling with the phosphorus nuclei was observed, due to the broadening of the signals observed when the phosphine was directly bound to a paramagnetic species. This finding is consistent with rather short electronic relaxation times and with a low spin density on the phosphorus atoms. The magnitudes of the shifts are fully comparable to those observed in the ^1H NMR spectrum of the cluster $[Fe_6(\mu_3\text{-}S)_8(PEt_3)_6]^+$, for which a spin-doublet ground state has been ascertained by magnetic measurements.[13]

The temperature dependence of the magnetic susceptibility, χ, for $[Co_6(\mu_3\text{-}S)_8(PEt_3)_6]BPh_4$ is shown in Figure 5 in the form χT vs T. A constant decrease of the effective magnetic moment, $\mu_{eff} = (8\chi T)^{1/2}$, from room temperature ($\mu_{eff} = 2.4\ \mu_B$) to 4.2 K ($\mu_{eff} = 1.8\ \mu_B$) is observed.

Discussion

We can assign formal charges of +3 to five cobalt atoms and +2 to one cobalt atom in the $[Co_6(\mu_3\text{-}S)_8(PEt_3)_6]BPh_4$ salt, assuming a −2 charge for the sulfur atoms. The cobalt(III) species must be diamagnetic, while cobalt(II) in an S_4P environment is expected to be low spin.

Since the crystals are triclinic, with only one site in the unit cell, there is no ambiguity in assigning the measured crystal **g** tensor to the molecule, remembering however that in any EPR experiment it is not possible to distinguish between molecules

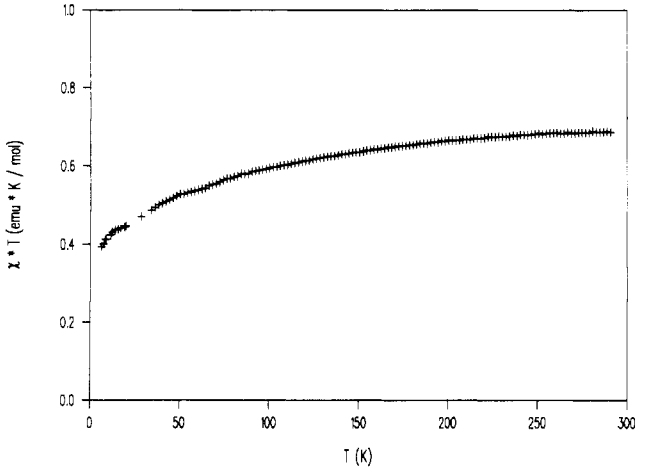

Figure 5. Temperature dependence of the magnetic susceptibility of $[Co_6(\mu_3\text{-}S)_8(PEt_3)_6]BPh_4$ in the form χT vs T.

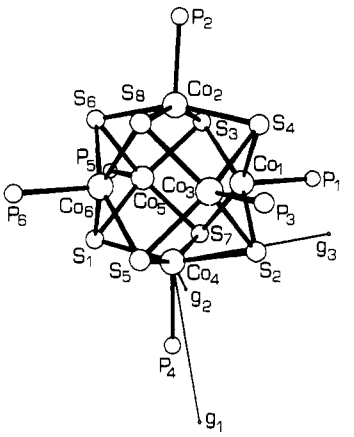

Figure 6. Orientation of the 4.2 K **g** tensor in the molecular frame of $[Co_6(\mu_3\text{-}S)_8(PEt_3)_6]BPh_4$.

related by a center of symmetry. The orientation of the **g** tensor measured at 4.2 K in the molecular frame is shown in Figure 6. The principal directions of **g** are close to bond directions centered on Co_4 or on the quasi-centrosymmetric Co_2: g_3 forms a 17° angle with the $Co_4\text{–}S_2$ bond, and g_1 forms an angle of 16° with the $Co_4\text{–}P_4$ bond. If we refer now to a right-handed metal-centered reference frame with the z axis parallel to the cobalt–phosphorus bond direction, we can write $g_x = 2.35$ (1), $g_y = 2.04$ (1), and $g_z = 1.95$ (1). Inspection of Table I shows that the x direction forms an angle of 35° with the X axis and the z direction makes an angle of 27° with the Y axis. The observed principal g values are comparable to the values observed in square planar[14,15] or square pyramidal[14,16] low-spin cobalt(II) complexes, and within the ligand field model, they are consistent with a ground Kramers doublet which is a linear combination of d_{xz}, d_{yz}, and d_{z^2}[17,18] metal orbitals, with a dominant contribution from d_{z^2}.[19] These results appear to be consistent with a localization of the unpaired electron on one of the six inequivalent metal centers, which reflects the low symmetry of the cluster. The electronic states of fully de-

(13) Snyder, B. S.; Holm, R. H. *Inorg. Chem.* **1990**, *29*, 274.

(14) Bencini, A.; Gatteschi, D. *Transition Metal Chemistry*; Melson, G. A., Figgis, B. N., Eds.; Marcel Dekker: New York, 1982; Vol. 8, p 1.

(15) (a) Maki, A. H.; Edelstein, N.; Davison, A.; Holm, R. H. *J. Am. Chem. Soc.* **1964**, *86*, 4580. (b) Kalbacher, B. J.; Bereman, R. D. *Inorg. Chem.* **1973**, *12*, 2997.

(16) (a) Nishida, Y.; Shimohori, H. *Bull. Chem. Soc. Jpn.* **1973**, *46*, 2406. (b) Nishida, Y.; Kida, S. *Bull. Chem. Soc. Jpn.* **1975**, *48*, 1045. (c) Gatteschi, D.; Ghilardi, C. A., Orlandini, A.; Sacconi, L. *Inorg. Chem.* **1978**, *17*, 3023.

(17) Daul, C.; Schlaepfer, C. W.; von Zelewsky, A. *Struct. Bonding (Berlin)* **1979**, *36*, 129.

(18) Ceulemans, A.; Debuyst, R.; Dejehet, F.; King, G. S. D.; Vanhecke, M.; Vanquickenborne, L. G. *J. Phys. Chem.* **1990**, *94*, 105.

(19) Bencini, A.; Ghilardi, C. A., Orlandini, A.; Midollini, S.; Zanchini, C. *J. Am. Chem. Soc.*, submitted for publication.

localized mixed-valence complexes are generally described[20,21] using linear combinations of antisymmetrized products of single-ion states (the so-called exchange-resonance multiplets). In the present case, the electronic wave functions which are relevant to the EPR spectra are linear combinations of products of five singlet states (on the cobalt(III) centers) and one doublet state (on the cobalt(II) center). It is clear that the expected value of the Zeeman operator applied to the ground-state function is equal to a spatial average over the different metal centers and the observed **g** tensor should be close to an average of the local **g** tensors. Since the symmetry of the whole cluster is not far from octahedral (for example, the six local z axes point two by two along three orthogonal directions), the **g** tensor computed in this way should be nearly isotropic and have the principal directions parallel to the cobalt–cobalt directions which correspond to the S_4 axes of the octahedron. Direct information on the extent of localization of the unpaired electron could be obtained from a measurement of hyperfine couplings. It is worth mentioning that no hyperfine or superhyperfine structure was observed even in the 4.2 K frozen-solution spectra. This behavior could be due to the an incomplete formation of the glass, probably caused by formation of aggregates of clusters, preventing a good magnetic dilution, as outlined in the Experimental Section. The overall appearance of the spectra is, however, solvent independent and the presence of six cobalt and six phosphorus atoms could cause a further broadening of the EPR signals as compared to those of mononuclear low-spin cobalt(II) complexes due to unresolved superhyperfine and transferred hyperfine interactions.[22]

The temperature dependence of the magnetic susceptibility showed a regular decrease of μ_{eff} from room temperature to 4.2 K. This behavior has already been observed in a cobalt(II) complex with a tetradentate Schiff base,[23] where the effective magnetic moment changed from $\mu_{eff} = 2.6\ \mu_B$ to $\mu_{eff} = 2.28\ \mu_B$ at 82 K, and was attributed to the thermal depopulation of excited quartet spin states, which are near the ground doublet state. Another possible mechanism which could produce the observed temperature variation of μ_{eff} is the existence of an antiferromagnetic interaction between the paramagnetic clusters. This interaction could be revealed by applying a Curie–Weiss law for the temperature dependence of the magnetic susceptibility of the type

$$\chi = C/(T - \Theta) \qquad (1)$$

where C is the Curie constant and Θ is the Weiss constant. No reasonable fit of the experimental data was obtained using the above expression, indicating that the magnetic interactions between paramagnetic centers, if any, cannot completely explain the observed magnetic behavior.

Since EPR spectroscopy is very sensitive to small magnetic effects, we have measured the angular dependence of the peak-to-peak line width, ΔB_{pp}, of the EPR signal. The angular dependence of ΔB_{pp} observed in the $YZ(bc)$ plane is similar to that already observed in linear magnetic chain or planar magnetic systems when the dipolar interactions dominate the exchange interactions and is characterized by a $(3\cos^2\theta - 1)$ type angular dependence, where θ is the angle between the static magnetic field and the chain axis or the perpendicular to the plane, respectively. This angular dependence is in fact characterized by a minimum line width at the "magic angle" $\theta = 54.7°$. The maximum of the line width was found, for magnetically one-dimensional compounds, along the chain axis. In the present case, the above model places this axis $\approx 10°$ from Y, i.e. close to the b crystallographic axis. In Figure 7, a projection of the structure of $[Co_6(\mu_3\text{-}S)_8(PEt_3)_6]BPh_4$ in the $bc(YZ)$ plane is shown. The arrangement

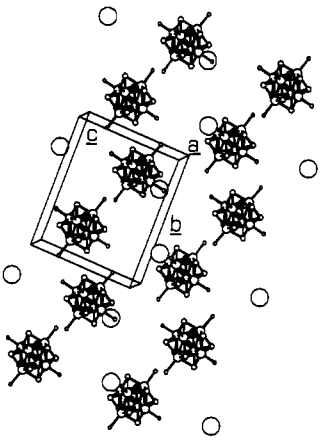

Figure 7. Projection of the structure of $[Co_6(\mu_3\text{-}S)_8(PEt_3)_6]BPh_4$ in the bc plane.

of the cobalt clusters along the b axis resembles an alternating linear chain, with each chain being separated by tetraphenylborate anions. The shorter distances between the cobalt atoms in two different molecules are 900 and 902 pm. Of course, much shorter distances occur between the phosphorus atoms and very close contacts are computed between the ethyl groups of triethylphosphine. The existence of magnetic dipolar and/or exchange interactions between the clusters in the solid state does not contrast with the crystal structure and can be a possible explanation of the observed angular dependence of the EPR line width. These interactions are however small, on the magnetic scale, and cannot explain the observed behavior of the magnetic susceptibility.

An angular dependence of ΔB_{pp} with a relative maximum could be also obtained by considering unresolved axial hyperfine splitting, depending on the relative values of the hyperfine parameters. It is well documented that both low-symmetry ligand field effects and covalency strongly influence the A and g values of low-spin cobalt(II) complexes, making impossible any spectral–structural correlations based only on these grounds. Literature data on $Co\text{–}S_4$ chromophores,[15] in which covalency is higher than in complexes with oxygen or nitrogen donor atoms, show A values in the range $(20\text{–}80) \times 10^{-4}\ cm^{-1}$, and we would expect similar hyperfine constants also for $[Co_6(\mu_3\text{-}S)_8(PEt_3)]BPh_4$, but no further discussion of their actual values is useful because of the lack of any experimental evidence. We can only try to analyze the angular dependence of the hyperfine coupling through sample calculations. The expressions needed to compute the second moment have been reported.[24,25] In general, however, the minimum line width is not computed at the magic angle from the maximum, which is observed along the direction of the maximum value of A. In many cases, an angular dependence with maximum and minimum 90° apart is computed, similar to that shown in Figure 3 in the planes perpendicular to Z and Y. By analogy with other five-coordinate square pyramidal low-spin cobalt(II) complexes,[17,18,20] the largest value of A should coincide with g_3, which is close to the $X(a^*)$ axis, so that the eventual effect of the hyperfine broadening of the EPR lines should be minimized in the $YZ(bc)$ plane. Due to the low symmetry of the coordination environment, the **A** tensor could be of course nonaxial and the principal directions of **A** could

(20) Anderson, P. W. In *Magnetism*; Rado, G. T., Suhl, H., Eds.; Academic Press: New York, 1963; Vol. 1, p 25.
(21) Tsukerblat, B. S.; Belinski, M. I.; Fainzil'berg, V. E. *Sov. Chem. Rev.* **1987**, *9*, 339.
(22) Owen, J.; Harris, E. A. In *Electon Spin Resonance*; Geshwind, S., Ed.; Plenum Press: New York, 1972; p 458.
(23) Reuveni, A.; Malatesta, V.; McGarvey, B. R. *Can. J. Chem.* **1977**, *55*, 70.
(24) Bencini, A.; Gatteschi, D. In *Electron Paramagnetic Resonance of Exchange Coupled Systems*; Springer-Verlag: Heidelberg, Germany, 1990.
(25) Equations 6.53–56 of ref 24, p 153, should read as follows (J. J. Borrás-Almenar, private communication):

$$M_2^{hyp} = (I(I+1)K^2(\theta))/(3g^2(\theta)) + (I(I+1)/6)[((A_\parallel{}^2A_\perp{}^2g^2(\theta))/K^2(\theta)) + A_\perp{}^2 + E^2(\theta)]$$

with

$$K^2(\theta) = A_\parallel{}^2g_\parallel{}^2\cos^2\theta + A_\perp{}^2g_\perp{}^2\sin^2\theta$$

$$g^2(\theta) = g_\parallel{}^2\cos^2\theta + g_\perp{}^2\sin^2\theta$$

$$E^2(\theta) = (A_\parallel{}^2 - A_\perp{}^2)g_\parallel g_\perp(\cos\theta)(\sin\theta)/(K^{1/2}(\theta)\, g^2(\theta))$$

Table II. Parameters Used in the Extended Hückel Calculations

atom	orbital type	VSIP, eV	c_1	ζ_1	c_2	ζ_2
Co	3d	-13.18	0.5746	5.55	0.6131	2.00
	4s	-9.21	1.00	2.00		
	4p	-5.29	1.00	2.00		
P	3s	-18.6	1.00	1.60		
	3p	-14.0	1.00	1.60		
S	3s	-20.0	1.00	1.82		
	3p	-13.3	1.00	1.82		
H	1s	-13.6	1.00	1.3		

be noncoincident with the principal directions of **g**. The noncoincidence of the **g** and **A** principal axes could also give rise to an angular dependence similar to that observed in the *YZ*(*bc*) plane. In low-spin cobalt(II) complexes, however, despite of the low symmetry of the chromophore, the **g** and **A** tensors have been generally found to be parallel within experimental error.[14,17,18] It is apparent at this point that a safe interpretation of the EPR data is not possible, but a reasonable explanation indicates the existence of intracluster interactions in the solid state. These interactions are probably too weak to have measurable effects on the magnetism of the complex. Unfortunately, we could not follow the temperature behavior of the line width, which could provide more information on the nature of the interaction.

The above discussion leads to the conclusion that the unpaired electron is localized on one of the six crystallographically inequivalent cobalt centers. Some comments however are still required to rationalize the high-temperature behavior of $[Co_6(\mu_3\text{-}S)_8(PEt_3)_6]BPh_4$. The disappearance of the EPR signal at temperatures higher than 20 K cannot be ascribed to the existence of intercluster interaction. In fact, this interaction should be minimized in fluid or frozen diluted solutions, which on the contrary have been found to be EPR silent. Also, sharp NMR signals were observed at room temperature, indicating a rather short electronic relaxation time. This behavior is at variance with that of mononuclear cobalt(II) complexes, which usually show good EPR spectra at room temperature. We suggest that the above observations could be explained by assuming a delocalization of the unpaired electron on the whole cluster for temperatures higher than 20 K. Due to the low symmetry of the cluster, it should in fact be possible that vibronic coupling gives rise to a temperature dependence of the localization of the electron, as already observed in other mixed-valence systems.[26]

In order to have a pictorial view of the energy level ordering in the $[Co_6(\mu_3\text{-}S)_8(PEt_3)_6]^+$ cation, we have performed extended Hückel calculations[27] on a model cation $[Co_6(\mu_3\text{-}S)_8(PH_3)_6]^+$ using the bond distances and angles seen in the crystal structure of $[Co_6(\mu_3\text{-}S)_8(PEt_3)_6]^+$, except for those involving the hydrogen atoms, which were placed tetrahedrally around each phosphorus 110 pm apart. The resulting energy level scheme is shown in Figure 8. The parameters used in the calculations are summarized in Table II. Employing this model, as well as any other molecular orbital model which uses a single Slater determinant, we overestimate the importance of electron delocalization, and we surely do not have a good description of the ground-state wave function; nevertheless, a number of conclusions regarding the electronic structure of the cluster can be drawn which can help to rationalize the experimental observations.

All energy levels up to -12 eV are occupied. The lowest lying levels, up to -22 eV, arise from nonbonding 3s orbitals of phosphorus and 1s orbitals of hydrogen; the 3s orbitals of sulfur, mainly nonbonding, are filled. Around -18 eV, a number of very closely spaced levels arising from phosphorus 3p and hydrogen 1s orbitals give rise to a narrow band, with a negligible contribution from the metals. The metal 3d orbitals contribute to the energy levels above -15.6 eV, which form a wide band of mixed sulfur–metal, and sometimes phosphorus, orbitals up to -12 eV. An energy gap

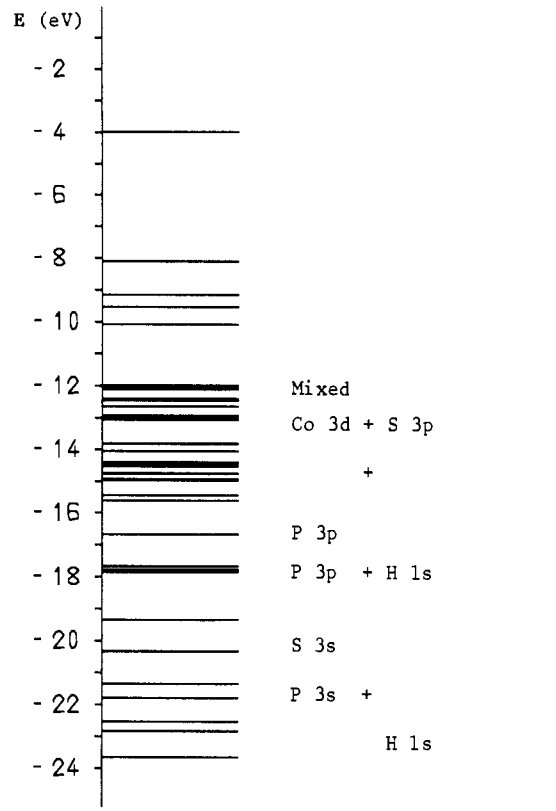

Figure 8. Energy level scheme for the model cation $[Co_6(\mu_3\text{-}S)_8(PH_3)_6]^+$ obtained from extended Hückel calculations using the parameters listed in Table II.

of 2 eV is computed between the top of the d band and the LUMOs. In order to have a simple view of the composition of the HOMOs and LUMOs, we can look at the metal 3d atomic orbitals of the cobalt atom lying on the *z* axis of the molecular reference frame. The d_{xz}, d_{yz}, and d_{z^2} orbitals form the quasi-degenerate HOMOs with energies in the range -12.10 to -11.99 eV. To these orbitals contribute also the sulfur 3p and phosphorus $3p_z$ orbitals, which interact with the MO having the largest d_{z^2} character. The LUMO orbitals, which have energies ranging from -10.1 to -9.5 eV, are essentially antibonding metal d_{z^2}–phosphorus $3p_z$ linear combinations. The relatively high HOMO–LUMO gap can thus be related to the antibonding interaction of the phosphorus atoms.

Although the above calculations are based on a semiempirical method which does not account for the interelectronic repulsion terms, some general comments can be made. The highest occupied orbitals are those expected for a low-spin square pyramidal cobalt complex, and if a localization occurs, they can explain the observed *g* values. Further, since the levels of the d band are very closely spaced in energy, a number of doublet states can arise, differing by one electron in the occupation of the molecular orbitals, which have comparable total energies. This manifold of states provides an efficient mechanism for the electronic relaxation which justifies the observed short electron relaxation time. The large HOMO–LUMO energy gap explains why the uncharged state of the $[Co_6(\mu_3\text{-}S)_8(PEt_3)_6]$ cluster was found to be diamagnetic, since a large exchange energy should be required to overcome this gap and to favor the triplet state as the ground state. The strong antibonding character of the LUMOs destabilizes the negative states and accounts for the fact that the existence of negative states has not yet been observed. From the LCAO composition of the molecular orbitals, we learn that the largest contribution of the phosphorus atoms is to the LUMOs; therefore a small spin density on phosphorus is anticipated, explaining why the NMR spectrum is well resolved at room temperature.

Further analysis of the relative stability of positively charged states in which more than one unpaired electron could be present demands the use of more sophisticated calculations that include

(26) Blondin, G.; Girerd, J. *J. Chem. Rev.* **1990**, *90*, 1359.
(27) Hoffmann, R.; Fujimoto, J. R.; Swenson, C.; Wan, C. C. *J. Am. Chem. Soc.* **1973**, *95*, 7644.

electron correlation, the application of which is presently under investigation.

Conclusion

The spectromagnetic properties of the $[Co_6(\mu_3\text{-}S)_8(PEt_3)_6]BPh_4$ cluster have been found to be rather complicated. At room temperature, the cluster is EPR silent and shows a rather exceptional well-resolved ^1H NMR spectrum. These properties suggest a delocalization of the unpaired electron over the whole molecule, even if the cobalt centers are crystallographically nonequivalent, which results in short relaxation times and a small spin density on the phosphorus atoms. The 4.2 K single-crystal EPR spectra are typical of a low-spin cobalt(II) complex, which can be formed if the unpaired electron localizes upon a decrease in temperature, and the angular dependence of the peak-to-peak line width of the EPR signal can indicate the existence of a magnetic interaction between the magnetic clusters, which are arranged in the solid state in an alternating linear chain in the *bc* plane. The observed magnetic behavior agrees with this interpretation. The low symmetry of the complex, while aiding us in the measurement of the molecular **g** tensor, prevented any deeper investigation of the intercluster interactions; also, the absence of a resolved hyperfine and/or superhyperfine splitting prevented a direct measurement of the localization of the unpaired electron. Since the extent of localization in mixed-valence complexes is the subject of active research and the above results show that magnetic and EPR measurements can yield useful information in this area, higher symmetry clusters are now under investigation.

The phosphine ligands prevent the formation of an extended structure with strong bonding interactions between the clusters, which have been observed in other oligonuclear compounds and are responsible for peculiar physical properties, but in a sense they modulate the electronic structure of the clusters through the creation of an energy gap inside the metal d band, influencing their redox and electron-transport properties. An analysis based on spin-unrestricted Xα–SW calculations[19] is in progress to study the relative stabilities of the degrees of oxidation of the cluster upon varying the number of electrons on the metals and to investigate the resulting spin structures.

Acknowledgment. Thanks are expressed to Prof. O. Kahn, Université de Paris Sud, for the magnetic measurements; to Prof. M. Verdaguer, Université P. et M. Curie, Paris, for his kind hospitality and helpful discussions; to Prof. D. Gatteschi, Università di Firenze, for his encouragement and suggestions; and to Mr F. Cecconi, for assistance in the chemical manipulations.

Registry No. $[Co_6(\mu_3\text{-}S)_8(PEt_3)_6]BPh_4$, 81289-54-5.

Contribution from the Department of Chemistry, University of Alberta, Edmonton, Alberta, Canada T6G 2G2

Kinetic Study of the Reaction of 3-Methylascorbic Acid with Aqueous Iron(III)

M. J. Sisley and R. B. Jordan*

Received December 26, 1991

The reactions of aqueous iron(III) with 3-methylascorbic acid (3-MeAsH) have been studied in dilute acid with iron(III) in excess in 1.0 M $LiClO_4/HClO_4$ at 25 °C. There is initial formation of a violet complex followed by much slower fading of the color. The formation of the violet color was studied by stopped-flow, and the iron(III) and H^+ dependence of the rate are consistent with the reaction of $(H_2O)_5FeOH^{2+}$ and 3-MeAsH with a rate constant of $(2.2 \pm 0.05) \times 10^3$ M^{-1} s^{-1}) to form $(H_2O)_5Fe(3\text{-}MeAs)^{2+}$. The slow step, which involves oxidation of 3-MeAsH and formation of iron(II), is strongly inhibited by iron(II), and the kinetics of the reaction have been studied with a pseudo-first-order excess of Fe^{2+}, with $[Fe^{2+}] \approx$ [3-MeAsH] and with no initial Fe^{2+}. For the latter two conditions, the absorbance–time profiles have been fitted by numerical integration of the appropriate second-order rate law. The oxidation follows two parallel pathways whose contributions depend on the $[Fe^{2+}]$. One pathway has an $[Fe^{2+}]^{-1}$ dependence and has an irreversible step prior to the transfer of the second electron. The other pathway, with an $[Fe^{2+}]^{-2}$ dependence, is analogous to that found previously for 1,2-dihydroxybenzoic acid. The analysis yields specific rate constants for the first electron transfer of 0.88 and 64 M^{-1} s^{-1} for $Fe(OH_2)_6^{3+}$ and $(H_2O)_5FeOH^{2+}$, respectively, and rate constant ratios for several intermediate steps.

Introduction

A recent study[1] of the reaction of aqueous iron(III) with ascorbic acid (**1**) has confirmed earlier observations[2] of the formation

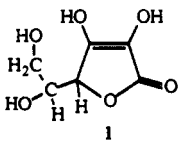

1

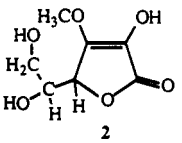

2

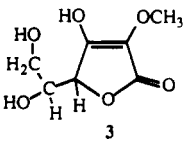

3

of a transient blue iron(III)–ascorbate intermediate and shown that this intermediate is oxidized by a second iron(III). It was also found[1] that the rate of formation of the blue species is unusually fast for substitution on $Fe(OH_2)_6^{3+}$ or $Fe(OH_2)_5OH^{2+}$. Observations during early preparative work[3] on the methyl derivatives of ascorbic acid indicated that 3-methylascorbic acid (**2**) (3-MeAsH) forms a more persistent blue complex than ascorbic acid, but the 2-methyl derivative (**3**) does not form a colored complex. These observations must have some relevance to the mode of coordination of ascorbate to aqueous iron(III). The fact that 3-methylascorbic acid is a much weaker acid ($pK_a = 7.9$)[4] than ascorbic acid ($pK_a = 4$) may also be helpful in differentiating the reactivity of the ionized forms in these systems. The acidity difference is consistent with the conclusion of Berger[5] that the 3-OH proton is the most acidic in ascorbic acid. However, it is then somewhat unexpected that the 3-methyl derivative also forms a blue iron(III) complex.

Some effort has been made to elucidate the organic products of the oxidation of 3-MeAsH, especially to determine if the methyl group is lost. Therefore it is pertinent to review briefly the information on the oxidation products of ascorbic acid. This problem has received considerable attention, but the literature is somewhat conflicting. Tolbert and Ward[6] have provided a review and new

(1) Xu, J.; Jordan, R. B. *Inorg. Chem.* **1990**, *29*, 4180.
(2) Laurence, G. S.; Ellis, K. J. *J. Chem. Soc., Chem. Commun.* **1972**, 1676. Keypour, H.; Silver, J.; Wilson, M. T.; Hamed, M. Y. *Inorg. Chim. Acta* **1986**, *125*, 97. Martinez, P.; Zulaga, J.; Uribe, D. *Z. Phys. Chem. (Munich)* **1987**, *268*, 105. Hynes, M. J.; Kelly, D. F. *J. Chem. Soc., Chem. Commun.* **1988**, 849.
(3) Haworth, W. N.; Hirst, E. L.; Smith, F. *J. Chem. Soc.* **1934**, 1556. Haworth, W. N.; Hirst, E. L. *Helv. Chim. Acta* **1934**, *17*, 520.
(4) Lu, P. W.; Lillard, D. W., Jr.; Seib, P. A.; Kramer, K. J.; Liang, Y.-T. *J. Agric. Food Chem.* **1984**, *32*, 21.
(5) Berger, S. *Tetrahedron* **1977**, *33*, 1587.

0020-1669/92/1331-2137$03.00/0